

Localized Strength Restoration of Aluminum 5083 with Ceramic Particles via Friction Stir Processing

A.E. Nolting¹, S. Larose², X. Cao², C. Munro¹,
R. Amos², B. Monsarrat² and P. Wanjara²

¹Defence R&D Canada – Atlantic Research Centre
CFB Halifax, Bldg D-20, Halifax, NS, B3K 5X5

²National Research Council Canada – Aerospace Research Center
5145 Decelles Ave., Montreal, PQ, H3T 2B2

CANADA

Allison.nolting@drdc-rddc.gc.ca

ABSTRACT

It has been well established that friction stir processing (FSP) can successfully be used to reduce flaws and repair defects, such as cracks and pores in a variety of alloys. When integrated with 3D robotic control, the FSP technology is a potential option for in-theatre repair or refurbishment of vehicle components. However, work-hardened aluminium alloys (AA), such as AA5083 can experience a degradation in strength during FSP due to recrystallization of the cold rolled microstructure, which may adversely affect the mechanical properties.

In an effort to combat the softening phenomenon for a repair solution, a procedure for incorporating ceramic particles into AA5083 using FSP technology was successfully developed in order to locally enhance the hardness and yield strength. A surface layer, drilled with a discontinuous pattern of holes, was first filled using alumina powder and then this area was friction stir processed with up to three repeated linear passes to manufacture a metal matrix composite (MMC) surface layer. Targeting a penetration depth of 5 mm and an average reinforcement fraction of 10 vol. % alumina particles, a homogeneous particle distribution was achieved without the formation of any visible internal or surface defects. The resulting MMC layer had average increases of 35% in microhardness and 25% in yield strength at a penalty of 50% in ductility, compared to the parent metal.

1.0 INTRODUCTION

Friction stir processing (FSP) is a surface modification technique derived from friction stir welding (FSW) that can be used for repair of surface cracks, reduction of casting porosity or microstructural modification [1]. In both FSP and FSW, a rotating tool is plunged into the surface of the workpiece and translated across the surface or seam, respectively. The FSP tool consists of a large diameter cylinder ‘shoulder’ with a protruding smaller diameter ‘pin’. The shoulder provides a downward force on the workpiece and generates frictional heat. The pin rotates in the workpiece, subjecting the local material to severe plastic deformation. This deformation, combined with the constraint applied by the shoulder of the tool, can repair cracks and close pore defects, resulting in improved mechanical properties and fatigue performance [1]. For instance, in cast materials, FSP breaks up the dendritic microstructure, creating refined uniaxial grains more typical of wrought materials [2,3]. These changes have been reported to improve strength, ductility and fatigue properties of cast materials [1,3]. Grain size refinement and the creation of high angle grain boundaries produced by FSP has been reported to result in

Localized Strength Restoration of Aluminum 5083 with Ceramic Particles via FSP

superplasticity of selected wrought materials, although it is typically accompanied with a decrease in strength [4,5]. The potential to remove defects in thick section parts with low distortions and improved microstructures, makes FSP an attractive technology for the repair and refurbishment of light alloys.

Unfortunately under some conditions, the application of FSP can cause a degradation of strength. The FSP of age hardenable aluminium alloys (AA), such as the 2xxx or 7xxx series can lead to dissolution of precipitates in the nugget, or growth of precipitates in the heat affected or thermo-mechanically processed zones, both of which can lead to decreased strength [4,1,6,7]. Challenges associated with heat treating the friction stir processed (FSPed) areas in isolation of the surrounding structure means that these zones can only be naturally aged. Recrystallization of work-hardened microstructures, which can occur during FSP, has also been shown to cause a decrease in strength [8]. It is thought that some of this strength can be regained by simultaneously incorporating ceramic particles into the nugget during FSP. The most effective methods of incorporating particles into the surface of a workpiece using FSP typically involve drilling holes or grooves into the surface of the workpiece, filling them with ceramic powders, and then dispersing the ceramics by passing the FSP tool over the area [9-13]. Development of FSP techniques for creating these metal matrix composite (MMC) surface layers has typically focused on increasing the wear properties [10,12,14] and hardness [9,10,11,14] but it has also been shown to improve the mechanical properties such as yield and ultimate strength [11,13] and ballistic resistance [12].

The FSPed MMCs could find an application in the repair and refurbishment of 5xxx series aluminium alloys. These alloys are used in military vehicles, such as the M113 armour personnel carriers, because of their high specific strength, good corrosion resistance and ballistic performance. They are not heat treatable alloys, but instead obtain their strength from cold working. As the use of conventional fusion based repair technologies would render considerable loss in strength, thereby defeating the intending application, 5xxx series alloys are not repairable. FSP can also cause a loss of strength in work-hardened AA5083 due to recrystallization [8]. Introducing ceramic particles to the FSPed nugget during repair could provide a viable option for in-theatre repair and refurbishment of AA5083 components, resulting in increased operational readiness of deployed land platforms. This study explores the use of ceramic particle reinforcements to strengthen AA5083-H131 during FSP, with the eventual goal of using the technique to develop a repair procedure for refurbishment of vehicles structures. The main objective of the current research study was to mature the technology readiness level (TRL) from concept (TRL 2) to validation in a laboratory environment (TRL 4) by demonstrating the feasibility of creating a 5 mm deep FSPed nugget with 10 vol.% of homogeneously distributed alumina particles and then performing laboratory experimentations to evaluate the performance through tensile and ballistic testing.

2.0 EXPERIMENTAL PROCEDURE

2.1 Fabrication of FSPed MMC Surface Layers

Base plate coupons for the FSP experiments were machined from conventionally processed armour-grade AA5083-H131 plate that had a thickness of 12.5 mm, a chemical composition as given in Table 2-1 and was manufactured according to MIL-DTL-46027. Typically, type AA5083 alloy plate is formed by hot rolling a cast ingot at temperatures in the range of 350-400°C [15]. As a non-heat treatable alloy, AA5083 is then strengthened through various degrees of strain hardening or cold working. The H131 designation indicates that the material has been cold worked to the final gauge, where the cold rolling has reduced the thickness of the plate from about 10% to about 30% (~20%), followed by deformation (e.g., stretching of the plate for flatness). The mechanical properties of the AA5083-H131 plate – yield strength of 327 MPa, ultimate tensile strength of 350 MPa and

Localized Strength Restoration of Aluminum 5083 with Ceramic Particles via FSP

elongation to failure of 11% – were obtained from a mill test certificate provided by Alcoa Inc.

Table 2-1: Chemical composition (wt%) of AA5083-H131 base plate, taken from the mill test certificate .

	Si	Fe	Cu	Mn	Mg	Cr	Zn	Ti	Al
AA5083	0.6	0.14	0.02	0.47	4.4	0.09	0.01	0.02	Balance

Commercially available ground calcinated alumina powder (Figure 2-1), purchased from Almatis Premium Alumina, was used for matrix enhancement. The fine alpha alumina crystallites were platelet-like in morphology and particle agglomeration was apparent. The particle size distribution as a function of particle frequency (Figure 2-2) was characterized with a Matec Applied Sciences Zeta-APS particle sizing apparatus, and 50% of the equivalent particle diameters were <0.2 μm, while the remaining 50% were between 3.5 and 4.75 μm. It is noteworthy that this characterization technique makes the assumption that particles are spherical, so the different sizes are not taking into account the aspect ratio of the particles.

A FSP procedure was developed at the National Research Council of Canada (NRC) to produce a continuous line of MMC on the surface of an AA5083-H131 plate. The target goals were to produce a layer with approximately 10 vol.% particles, 5 mm deep, with a homogeneous particle distribution in the AA5083-H131 matrix. To accomplish this, a single row of holes were drilled into the surface of a 12.7 mm thick AA5083-H131 plate and filled with alumina powder prior to subjecting it to one, two or three passes with a FSP tool, as illustrated in Figure 2-3. It is noteworthy that the size and spacing of the holes were selected to create the targeted 10 vol.% particles.

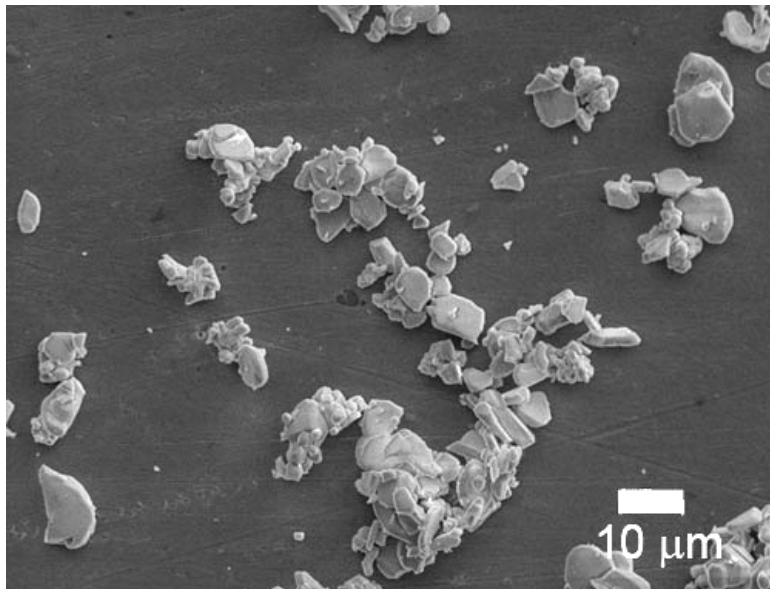


Figure 2-1: Morphology of typical Al₂O₃ Particles

FSP trials were performed using a MTS I-STIR FSW system operated in position control mode (Figure 2-4). All FSP passes were conducted in the same direction using a tool manufactured from H13 hardened steel. The tilt

Localized Strength Restoration of Aluminum 5083 with Ceramic Particles via FSP

angle was set at 3° with respect to the normal of the target surface. FSPed MMC surface layers with various combinations of the process parameters, including tool rotational speed (500 or 2000 rpm), tool travel speed (0.1, 0.5 or 1.0 mm/s), hole centre spacing (close hole spacing of 1S and far hole spacing of 2S) and the number of passes (1, 2 or 3), were fabricated and evaluated with radiography, contrast analysis and conventional metallographic techniques.

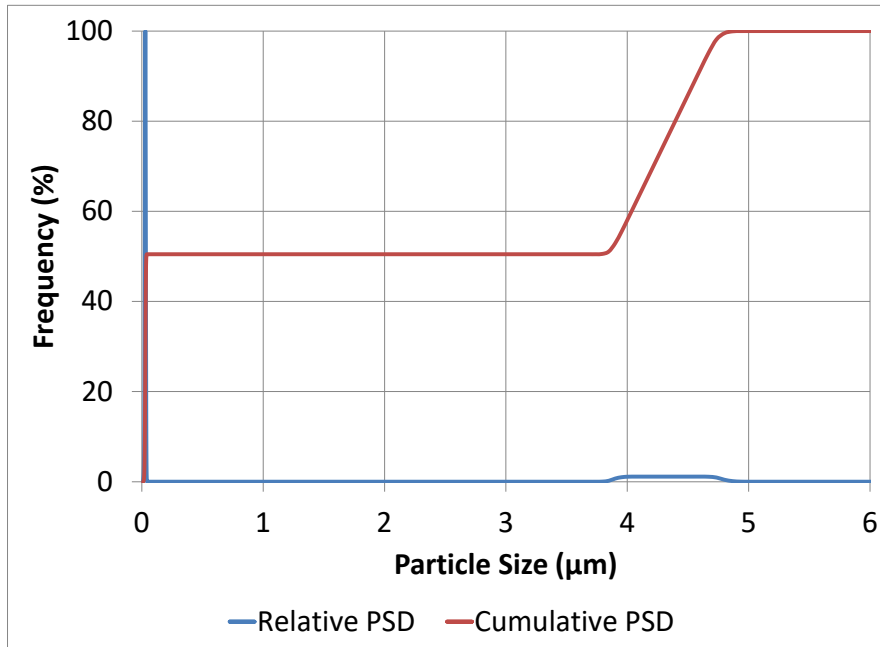


Figure 2-2: Al₂O₃ Particle Size Distribution

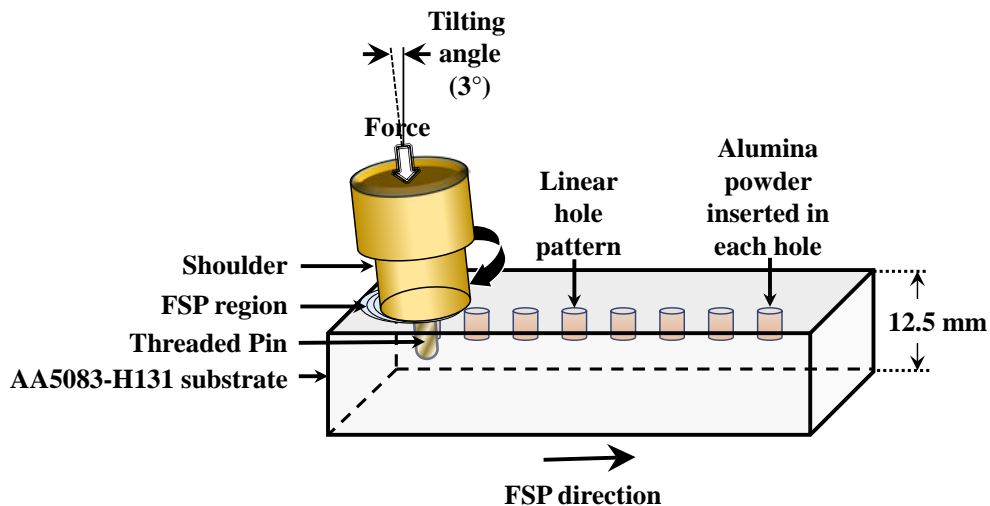


Figure 2-3: Process for manufacturing a FSPed MMC surface layer

Localized Strength Restoration of Aluminum 5083 with Ceramic Particles via FSP



Figure 2-4: MTS I-STIR friction stir welding system used to fabricate FSP MMCs

2.2 Material Evaluation

Radiography was used to quickly assess the homogeneity of the FSPed MMCs and to screen for internal defects. The film radiographs were digitized, compensated for variation in brightness, and analysed using MaZda [16-18] software to objectively evaluate the image contrast. A number between 0 and 1 was assigned to each radiograph, where 1 was a perfectly homogeneous image and 0 was essentially checker board of pure white and pure black pixels. Materials were selected for conventional metallographic homogeneity analysis based on the results of the contrast analysis. Transverse cross sections were taken from the specimens, mounted in Bakelite pucks and polished to a 0.25 μm finish. Images of the microstructure were taken with a Leica DMI 3000M optical microscope equipped with Clemex Technologies Inc. automated control hardware. To capture the entire cross section of the nugget, multiple images were taken and stitched together using the Clemex Technologies Vision Lite Software (Version 6.0.034). For some of the FSPed MMCs, mosaic images were also taken on longitudinal cross sections extracted from the centre line of the FSPed nugget.

Vickers micro-hardness mapping of select transverse cross sections was conducted in accordance to ASTM E384-10 [19] on a Clemex Technologies Inc. MMT-X7 Microhardness Tester with a 100 gf load and 10 second dwell time. Measurements were taken in a grid pattern with 300 μm spacing in both the x and y directions. Contour plots of the microhardness results were produced using Golden Software Inc. Surfer Version 9.2.397 Surface Mapping Software.

To assess the relative mechanical performance of the base plate and the FSPed MMC surface layer, stress-displacement curves were measured on subsized hourglass specimens (Figure 2-5) using a Scanning Electron Microscope (SEM) tensile stage with a 2 kN load cell. Displacement was measured by the separation of the grips and thus captured the deformation of the entire gage length. An hourglass configuration was chosen in an attempt to force failure at the centre of the specimen where the SEM could capture images of the damage accumulation. The specimens were oriented such that the loading direction was perpendicular to the length of the

Localized Strength Restoration of Aluminum 5083 with Ceramic Particles via FSP

FSPed zone, and the centre of the specimen was near the centreline of the FSPed nugget. Specimens were extracted by Electrical Discharge Machining (EDM) from three random locations along the length of the FSP pass (labelled 1, 2 and 3). As the specimens were only 1 mm thick and the FSPed nugget was 5 mm deep, three specimens were extracted from the nugget at each location. The depth of the specimens was represented by an A, B or C, with A being the specimen closest to the surface and C being closest to the bottom of the nugget. Tensile specimens were identified by their location along the length of the FSPed pass and extraction depth, for example 1C was taken from location 1 and was the specimen farthest from the top surface. The reported stress values were calculated from the applied load and the minimum cross sectional area of the specimen.

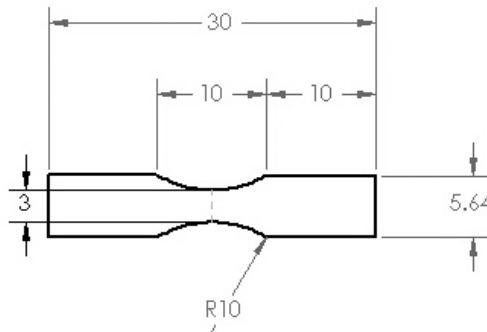


**Figure 2-5: Dimensions of the stress-displacement specimens (all dimensions in mm).
Specimen thickness = 1 mm**

V_{50} ballistic testing, which identifies the velocity at which 50% of projectiles penetrate a target, was conducted at Biokinetics and Associates Ltd on two FSPed MMC plates (2A and 2B) and one monolithic AA5083-H131 plate. The tests were conducted in accordance to MIL-STD-662F, using 7.62×39 mm FSP-17 CDN (DREV 97080605) fragment simulating projectiles and an obliquity angle of 0° . The location of the FSPed nugget was marked on the strike face of the plates to provide a target for aiming the projectiles.

3.0 RESULTS AND DISCUSSION

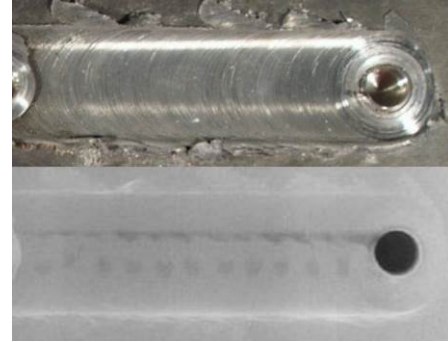
The FSPed MMCs with varying degrees of homogeneity and quality of surface finish are shown in Figure 3-1. In the radiographs, areas with lower density or of lower thickness (such as the tool exit holes) appear darker on the images. Surface breaking and internal voids have a lower density than the aluminium plate and will appear as dark areas on the radiographs. Figure 3-1a shows a radiograph with dark regions caused by surface breaking and internal voids, and represents the poorest combination of processing parameters tested. The FSPed MMC shown in Figure 3-1b has a good surface finish (i.e no surface breaking voids), but the radiograph shows periodic dark areas, which were confirmed by destructive metallography to be pockets of compacted powder and voids. Figure 3-1c shows another FSPed MMC with a good surface finish. The accompanying radiograph shows very little contrast, even between the FSPed nugget and the base plate, indicating the absence of porosity. The dispersion of alumina particles in the nugget should cause a change in density compared to the base plate. As the radiographs appear homogeneous between the FSPed nugget and the base plate, the radiographic procedure used to evaluate the FSPed MMCs was not sensitive enough to elucidated particle density of well incorporated particles. Figure 3-2 shows the cross section of two FSPed MMCs that received similar values in the contrast analysis. The cross section in Figure 3-2a is clearly more homogeneous than that in Figure 3-2b, yet contrast

Localized Strength Restoration of Aluminum 5083 with Ceramic Particles via FSP

analysis of the radiographs assessed the latter as being more homogeneous. While clearly inhomogeneous, the image in Figure 3-2b is stratified, and since the radiograph displays the average density through the thickness of the plate, the inhomogeneity may have been masked. Comparison of the radiographs with destructive metallography indicates that radiography is an adequate technique to screen for voids or pockets of unincorporated particles, but it is not effective at evaluating the homogeneity of well dispersed particles.



a) Tool rotational speed 2000 rpm,
tool travel speed 0.5 mm/s,
hole centre spacing 1S, 3 passes
Contrast Analysis = 0.49



b) Tool rotational speed 2000 rpm,
tool travel speed 0.1 mm/s,
hole centre spacing 2S, 1 pass
Contrast Analysis = 0.57



c) Tool rotational speed 500 rpm, tool travel speed 0.5 mm/s,
hole centre spacing 1S, 2 passes
Contrast Analysis = 0.93

Figure 3-1. Examples of surface finish and contrast analysis: a) poor surface finish and extensive porosity, b) good surface finish and poor homogeneity, and c) good surface finish and good homogeneity

Localized Strength Restoration of Aluminum 5083 with Ceramic Particles via FSP


a) Tool rotational speed 500 rpm
 tool travel speed 0.5 mm/s
 hole centre spacing 1S, 2 passes
 Contrast Analysis = 0.93



b) Tool rotational speed 500 rpm
 tool travel speed 1 mm/s
 hole centre spacing 2S, 2 passes
 Contrast Analysis = 0.93

Figure 3-2. Two FSPed MMCs with similar contrast analysis values, illustrating how radiography failed to discern non-homogeneous 'layering' in some of the FSPed MMCs:

- a) a cross section with reasonably homogeneous particle distribution,
 b) a cross section with striated particle distribution

Based on the radiography contrast analysis, FSPed MMCs were selected for metallurgical and microhardness evaluation. For instance, in Figure 3-3, the transverse and longitudinal cross sections illustrate the effect of multiple passes on particle dispersion of MMCs FSPed using conditions of close hole spacing (1S), travel speed of 0.5 mm/s and rotational speed of 500 rpm. After one pass, particles have been dispersed throughout the entire FSPed nugget, but there are areas of higher concentration near the edges and top of the nugget. The longitudinal cross section shows higher concentrations of particles corresponding to the spacing of the drilled holes. By the third pass, the transverse cross section is mostly homogeneous, with only a small indication of the circumferential onion ring pattern typical of FSPed nuggets. The longitudinal cross section appears to have a slight amount of striation, but is reasonably homogeneous.

Increased homogeneity with increasing number of passes is also evident in the contour plots of the microhardness data, as shown in Figure 3-4 for the MMCs FSPed with close hole spacing (1S), travel speed of 0.5 mm/s and rotational speed of 500 rpm. The contour plot of a single pass shows values as high as 140 HV in areas with high volume fractions of particles, and values similar to the base plate where there are few particles. By the third pass, the majority of the microhardness values in the FSPed nugget are between 95 to 115 HV. This represents an increase in the microhardness compared to the base plate, which was measured to be 70 to 85 HV.

The FSPed MMCs with close hole spacing (1S), travel speed of 0.5 mm/s and rotational speed of 500 rpm and 2 passes were found to have reasonably homogeneous particle distributions and, as such, were selected for tensile and ballistic testing. Stress-displacement curves for FSPed MMCs and the base AA5083-H131 are plotted in Figure 3-5. All of the specimens failed in the gage section near the minimum cross section. The tensile test results show that the FSPed MMCs have higher yield stress, but lower ductility than the AA5083-H131 base plate. While the behaviour of the base plate is consistent, the stress-displacement curves for the FSPed MMC show two distinct behaviours. Specimens 3C and 1A had ultimate strengths >350 MPa, while specimens 1B, 2A and 3B had similar ultimate strength to the base AA5083-H131, in the range of 250-300 MPa. The stress-displacement curves demonstrate that strength loss from recrystallisation of the strain-hardened AA5083-H131 microstructure can be regained by introducing ceramic particles into the FSPed nugget. However, the strength gain comes at the cost of lower ductility.

Localized Strength Restoration of Aluminum 5083 with Ceramic Particles via FSP

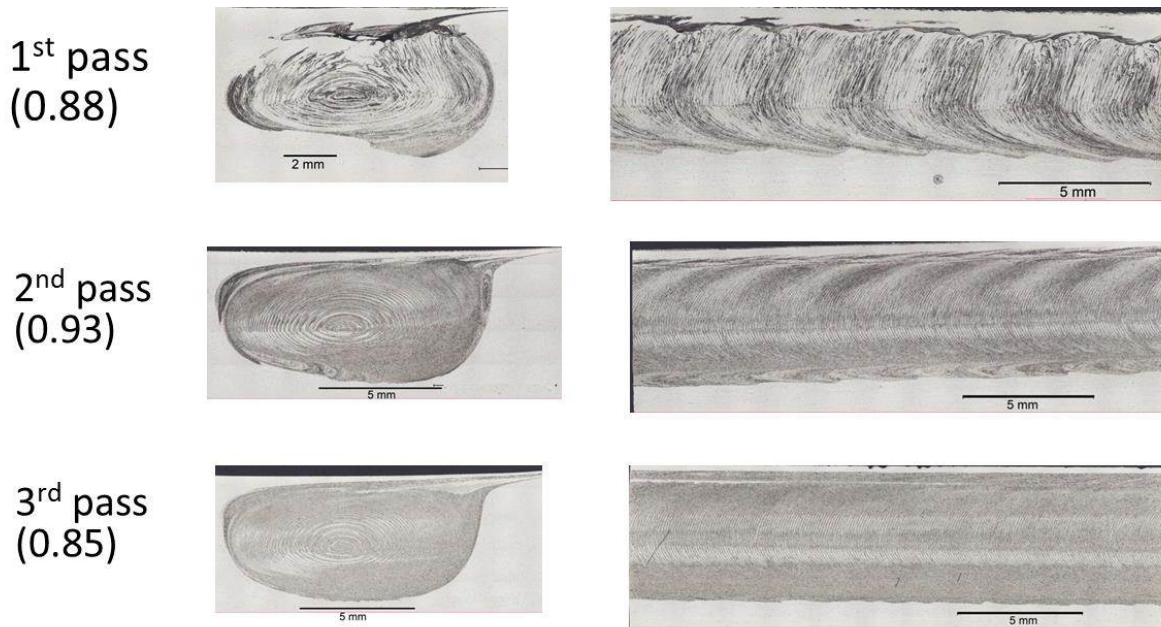


Figure 3-3: Transverse and longitudinal cross sections of FSP MMC: Tool rotational speed 500 rpm, travel speed 0.5 mm/s and close hole centre spacing (1S). Contrast analysis results presented in parenthesis

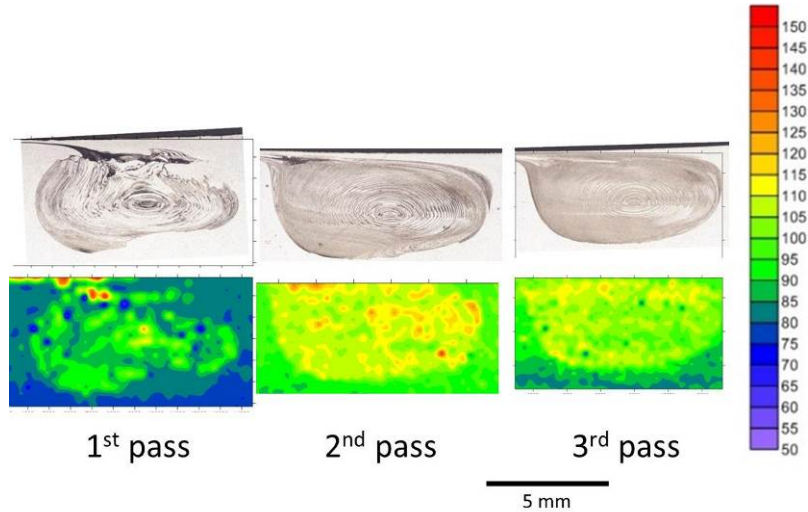


Figure 3-4. Microhardness plots of cross sections: Tool rotational speed 500 rpm, travel speed 0.5 mm/s and close hole centre spacing (1S)

Further research is required to understand the cause of the varied stress-displacement response of the FSPed MMCs, as the limited data set does not show a trend with respect to location or the depth of the specimens. It should be noted that the suffix in the specimen nomenclature only denotes the relative location of the specimens with respect to depth. Variation in the amount of material skimmed from the top of the plate, the thickness of the

Localized Strength Restoration of Aluminum 5083 with Ceramic Particles via FSP

EDM cuts and specimen thickness may have affected the location of the specimens within the FSPed nugget. As such, two specimens taken from the “top” layer may not have been extracted from the exact same location planned within the nugget, and the varying material properties may indeed be related to the location of the specimens in the FSPed nugget. Nonetheless, Figure 3-5 demonstrates that the addition of ceramic particles can enhance or maintain the strength of AA5083-H131 making it a viable option for the repair and refurbishment of components.

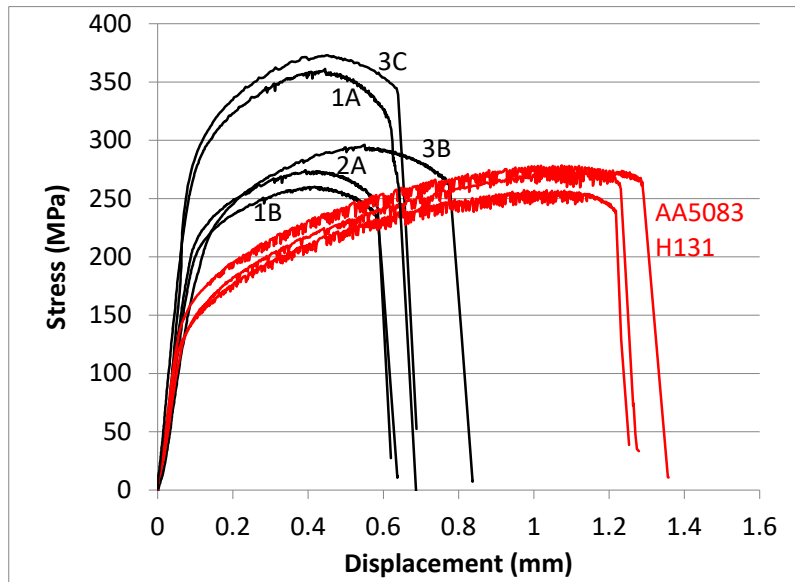


Figure 3-5. Stress-Displacement curves for FSP MMC AA5083 and base alloy A5083-H131

The incorporation of ceramic particles into the AA5083 plate resulted in an increase in hardness, which would be expected to lead to improved ballistic performance. The V_{50} calculated for the monolithic AA5083-H131 plate was 1200 m/s. Although both plates were processed with the same FSPed MMC parameters, separate V_{50} values of 1005 and 1008 m/s were calculated for plates 2A and 2B, respectively. Due mostly to the location of the shot with respect to the FSPed zone or a previous shot, only 4 and 6 data points were used in the V_{50} calculation for plates 2A and 2B, respectively. The results of the ballistic testing suggest that the FSPed MMC have inferior performance to the monolithic AA5083-H131 alloy. It can be seen in Figure 3-6 that the projectiles were similar in size to the FSPed nugget, and as such interacted with not only the FSPed MMC, but the adjacent thermo-mechanically affected zones, and possibly some monolithic AA5083-H131 alloy. In addition, ballistic performance is not solely a function of hardness, and it is possible that the decreased ductility of the FSPed MMC counteracted any positive effect from the increased hardness. The experiment should be repeated with smaller projectiles, or a larger FSPed MMC zone to ensure that only the FSPed MMC material is being evaluated. Development of 2D FSPed MMC areas could provide more appropriate plates for ballistic testing.

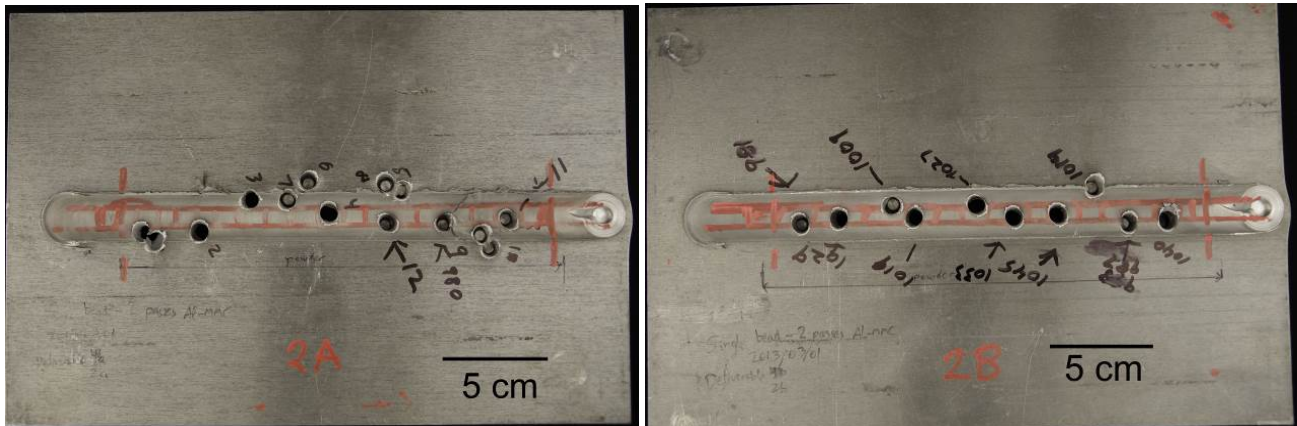


Figure 3-6. Tested FSP MMC ballistic plates

4.0 APPLICATIONS

Friction stir processes are valuable tools for the repair and refurbishment of damaged components when the processes maintain or enhance the properties of the original item. For some alloys, such as strain hardened aluminium, friction stir processes can cause recrystallization leading to decreased strength [8]. This paper has demonstrated that incorporating ceramic particles into the material during FSP can maintain or enhance the strength of FSPed AA5083-H131 plate. As this alloy is used in many aging military vehicle applications, the ability to repair or refurbish existing parts could have a positive effect on both the cost of maintenance and the availability of the platforms when replacement parts are no longer commercial-off-the-shelf or military-off-the-shelf items.

The increased hardness of FSPed MMCs can improve wear resistance in the processed area if the surface layer without particles is machined away after FSPing. It is also likely that mechanical properties could be tailored to specific applications by changing the type or volume fraction of the reinforcing particles. Future work could also focus on how to incorporate ceramic particles when conducting FSP -of precipitation-hardened alloys that also exhibit softening in the weld nugget and thermo-mechanically affected zones stemming from changes occurring local to the precipitation state.

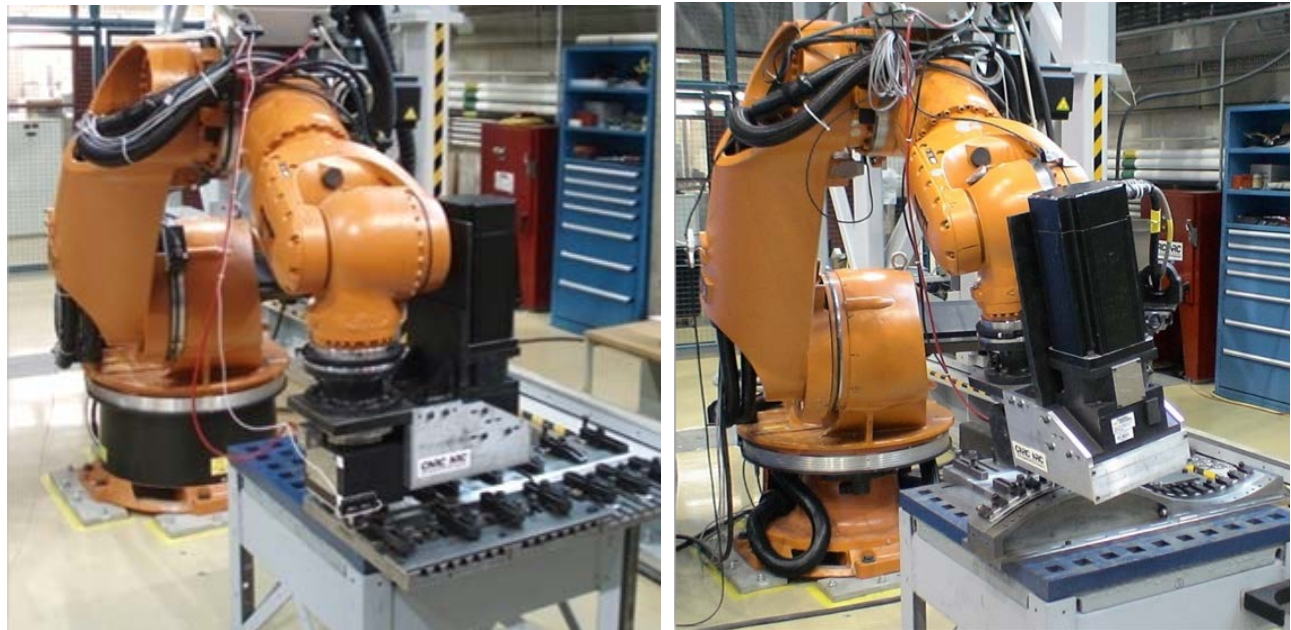
However, in order to be truly effective as a maintenance tool, the FSP process must be able to process large areas and contoured parts. Since the early 2000s, several research groups have demonstrated the significant potential of polyarticulated robots for the industrialization of the FSW process in planar and 3D applications [20-24]. In order to maximize the benefits of high reconfigurability, 3D capability, large workspace and low acquisition cost of off-the-shelf industrial robots, these studies have proposed a variety of technological platforms involving real-time process control technologies resorting to hybrid force/position control laws coupled with various feedback loops for accuracy management. Although the aforementioned references show the significant potential of using robotic technological platforms for FSP applications, the art in the field also demonstrate that such a migration should follow a certain continuum of R&D activities in order to ensure a successful in-theatre repair deployment. The main phases of this R&D continuum are described hereafter.

- Phase 1:** The first step of this sequence is to determine the most appropriate robot model, and potentially the linear unit on which the robot is mounted, based upon a priori knowledge of i) the maximum dimensions and shape characteristics of the vehicle components to be repaired or refurbished and ii) the maximum FSP parameters to be used for these operations as well as iii) the anticipated FSP trajectory patterns. This first step is achieved through careful analysis of the available operational windows of the candidate industrial robot(s). The operational window of a given robot model is delimited by its so-called kinetostatic capability. The latter combines both the robot's kinematic reachability, depending on the robot geometry and range of motion of its joints, and its static capability that is dependent on the maximal available continuous torques in the robot actuators. Contrary to gantry systems typically used in friction stir applications, the kinetostatic capability is highly nonlinear and non-homogeneous throughout the envelope of polyarticulated robots due to the coupling of the joint motion when generating a desired Cartesian path. A thorough description of the operational window of polyarticulated robots, supported by detailed schematics, has been provided by some of the authors in [25].
- Phase 2:** Once a robot model has been chosen, be it rail-mounted or not, depending on the maximum dimensions of the family of components considered, the next step is to design a layout of the robotic workcell meeting the application requirements. This implies the design of an appropriate fixture and clamping method, as well as defining its position and orientation with respect to the robot mounting base. This design should ensure that full reachability of the robot end-of-arm tooling is guaranteed throughout the FSP trajectories without crossing any robot kinematic singularity, whilst allowing the robot to sustain the process forces. Other criteria may be taken into consideration during this phase such as the quality of the ergonomics of the operator's postures when performing the setup of the components in the fixture. The reader is referred to [24] and [25] for detailed explanations on both the methodology and the underlying computational algorithms in order to achieve this design exercise in the case of planar aluminium components. The extension of this methodology and associated computational algorithms to the case of a large 3D aluminium component is provided in [26].
- Phase 3:** Having identified a robotic scenario under which the operational window is compatible with the FSP conditions can then allow the detailed design of a digital twin of the workcell layout in a CAD environment incorporating a robot simulation capability. At the end of this phase, this digital twin should include high fidelity engineering models of the selected robot, FSP spindle, tools, fixture and clamping devices. This phase can be employed for cycle-time analysis, budgetary estimation of the costs and the return on investment. More importantly, this simulation and verification phase can mitigate the risks associated with procuring and implementing the FSP workcell for the targeted application. Potential collisions between objects can for instance be detected through a simulation of robot motions. The ergonomics of operator's postures can be validated during this activity as well.
- Phase 4:** Once the robot, FSP spindle, tools, fixture and clamping devices have been procured and/or manufactured, they are assembled in conformity with the layout of the aforementioned digital twin. The system should also incorporate a set of technologies for robust real-time robotic FSP process control allowing the achievement of a very stable control of the forge force with maximal tracking reactivity and minimized overshoot. This real-time control unit should also allow a stable management of the transient phase in order to generate very smooth transitions between the tool plunge and FSP phases. In addition to real-time process control, system monitoring features should

Localized Strength Restoration of Aluminum 5083 with Ceramic Particles via FSP

be incorporated in the process control module in order to monitor all system critical signals such as currents on all robot axes or spindle RPM and torque. In the event of any abnormality, the system should automatically trigger failure recovery modes in order to achieve a high degree of robustness during in-theatre FSP operations. A relevant accuracy management strategy should also be included in order to ensure that the robot path generation occurs within tolerances. It is noteworthy that such an integration activity should also guarantee full compliance with all applicable robotic safety standards. The reader is referred to [24] for a detailed description of a set of technologies that were recently developed by the NRC in order to industrialize a robotic FSW platform. At the time of preparation of this paper, this robotic system, in production since 2015, had allowed the successful refurbishing of more than 18.000 1.76m x 1m aluminium components at this NRC client's facility located in the greater Montreal region.

Several examples of robotic FSW scenarios, synthesised using the aforementioned methodology in the case of both planar and 3D applications, are illustrated in Figs 4-1 and 4-2.



(a)

(b)

Figure 4-1. Robotic FSW workcell incorporating a floor-mounted KUKA KR500-MT industrial robot, a 10kW spindle and a fixturing table positioned to provide a viable operational window as per the results of the analysis presented in [25]. (a) Robot performing a 1m-long weld in a planar application. (b) Robot performing a FSW assembly along a 3D convex-concave path.

Localized Strength Restoration of Aluminum 5083 with Ceramic Particles via FSP



Figure 4-2. Robotic FSW workcell incorporating a KUKA KR500-MT industrial robot mounted on a high accuracy linear unit with 5m nominal travel. In this application, the robot is performing a 1m-long weld in a planar application by maximizing contributions of rail translations during synchronized robot/rail motions.

5.0 CONCLUSIONS

A friction stir processing technique was developed that could achieve the target goals of dispersing 10 vol. % particles into a 5 mm deep FSPed nugget. A homogeneous distribution was achieved in 2 to 3 passes. Radiography was demonstrated to be an effective tool for screening void defects, but it was unable to identify areas of higher particle concentration in the FSPed nugget.

The microhardness range increased from 70 - 85 HV in the base plate to 95 - 115 HV in an FSPed nugget with homogeneous particle distribution. Individual microhardness values above 140 HV were recorded in areas with high volume fraction particles in inhomogeneous FSPed nuggets. It was demonstrated that the addition of ceramic particles strengthened the material, making it a viable option for repair of structural components. The V_{50} performance of the FSPed MMC using 7.62×39 mm FSP-17 CDN (DREV 97080605) fragment simulating projectiles was inferior to the monolithic AA5083-H131. However the relative sizes of the FSPed nugget and the projectile meant that the projectile interacted not only with the FSPed MMC, but also with the thermo-mechanically affected zone and potentially the monolithic plate. Additional testing is required to develop a better understanding of the ballistic performance of the FSPed MMC.

Also, the main phases of the R&D activities required to migrate this FSP technique from laboratory level to in-theatre repair deployment using polyarticulated robots were presented. This continuum of activities has been formulated to ensure the deployment of a robotic FSP scenario presenting a set of specifications to accommodate i) the maximum dimensions and shape characteristics of the vehicle components to be repaired or refurbished and ii) the maximum FSP parameters to be used for these operations as well as iii) the anticipated FSP trajectory patterns.

Future research should focus on understanding the cause of the variation in mechanical properties over the FSP path and with depth, how a target volume fraction of particles affects the strength and ductility of the FSPed

MMCs, development of 2D FSPed areas and further automation of the friction stir process.

6.0 ACKNOWLEDGMENTS

This work was supported by the Technology Invest Fund of Defence Research and Development Canada (DRDC) and the Air, Defence and Systems (ADS) Program of the National Research Council of Canada (NRC). The authors are grateful to M. Guerin (NRC) for supporting the FSP experiments, and Nancy Hervé and Kyle Avery (DRDC) for their support to the metallurgical and mechanical testing.

7.0 REFERENCES

- [1] *Friction Stir Welding and Processing*, 2007, ASM International, Materials Park Ohio, Editors R.S. Mishra and M.W. Mahoney.
- [2] M.D. Fuller, S. Swaminathan, A.P. Zhilyaev, T.R. McNelley, *Microstructural transformations and mechanical properties of cast Ni Al Bronze: Effects of fusion welding and friction stir processing*, Materials Science Engineering A, vol 463, 2007, pp. 128-137.
- [3] C.B. Fuller, M.W. Mahoney, W.H. Bingel, M. Calabrese and B. London, *Tensile and fatigue properties of friction stir processed Ni Al Bronze*, Materials Science Forum, vols 539-543, 2007, pp. 3751-3756.
- [4] I. Charit and R.S. Mishra, *High strain rate superplasticity in a commercial 2024 Al alloy via friction stir processing*, Materials Science & Engineering A, vol 359, 2003, pp. 290-296.
- [5] F.C. Liu and Z.Y. Ma, *Achieving exceptionally high superplasticity at high strain rates in a micrograined Al-Mg-Sc alloy produced by friction stir processing*, Scripta Materialia, vol 59, 2008, pp. 882-885.
- [6] P.S. De and R.S. Mishra, *Friction stir welding of precipitation strengthened aluminium alloys: scope and challenges*, Science and Technology of Welding and Joining, vol 16(4), 2011, pp. 343-347.
- [7] R. A. Behnagh, M.K. Besharati Givi and M. Akbari, *Mechanical properties, corrosion resistance and microstructural changes during friction stir processing of 5083 aluminum rolled plates*, Materials and Manufacturing Processes, vol 27, 2012, 636-640.
- [8] D. Rao, K. Huber, J. Heerens, J.F. dos Santos, N. Huber, *Asymmetric mechanical properties and tensile behaviour prediction of aluminium alloy 5083 friction stir welding joints*, Materials Science & Engineering A, vol 565, 2013, pp. 44-50.
- [9] W. Wang, Q-Y Shi, P. Liu, H-k Li and T. Li, *A Novel way to produce bulk SiCp reinforced aluminium metal matrix composites by friction stir processing*, Journal of Materials Processing Technology, vol 209, 2009, pp. 2099-2103.

- [10] A. Shafiei-Zarghani, S.F. Kashani-Bozorg and A. Zarei-Hanzaki, *Microstructures and mechanical properties of Al/Al₂O₃ surface nano-composite layer produced by friction stir processing*, *Materials Engineering A*, vol 500, 2009, pp. 84-91.
- [11] C.J. Lee, J.C. Huang and P.J. Hsieh, *Mg based nano-composites fabricated by friction stir processing*, *Scripta Materialia*, vol 54, 2006, pp. 1415-1420.
- [12] I. Sudhakar, V. Madhu, G. Madhusudhan Reddy and K. Srinivasa Rao, *Enhancement of wear and ballistic resistance of armour grade AA7075 aluminum alloy using friction stir processing*, *Defence Technology*, vol 11, 2015, pp. 10-17.
- [13] S. Sahraeinejad, H. Izadi, M. Haghshenas and A.P. Gerlich, *Fabrication of metal matrix composites by friction stir processing with different particles and processing parameters*, *Materials Science & Engineering A*, vol 626, 2015, pp. 505-513.
- [14] R. Abdi Behnagh, M.K. Besharanti Givi, M. Akbari, *Mechanical properties, corrosion resistance, and microstructural changes during friction stir processing of 5083 aluminum rolled plates*, *Materials and Manufacturing Processes*, vol 27(6), 2012, pp. 636-640.
- [15] P.J. Hazell, *Armour: Materials, Theory, and Design*, CRC Press, 2015, pp. 190.
- [16] MaZda Image Texture Analysis Software, www.eletel.p.lodz.pl/programy/mazda/, last accessed January 23 2018.
- [17] M. Strzelecki, P. Szczepinski, A. Materka, A. Klepaczko, *A software tool for automatic classification and segmentation of 2d/3d medical images*, *Nuclear Instruments & Methods in Physics Research A*, vol 702, 2013, pp. 137-140.
- [18] P. Szczepinski, M. Strzelecki, A. Materka, A. Klepaczko, *MaZda-a software package for image texture analysis*, *Computer Methods and Programs in Biomedicine*, vol 94(1), 2009, pp. 66-76.
- [19] *ASTM E384-10 Standard test method for microindentation hardness of materials*, Vol 3.01, ASTM International, 2011 Annual book of ASTM Standards.
- [20] C. Smith, J. Hinrichs and W. Crusan, *Robotic friction stir welding: state of the art*, *Proceedings of the 4th International Symposium on Friction Stir Welding*, Salt Lake City, USA, 2003.
- [21] G. E. Cook, R. Crawford, D. E. Clark and A. M. Strauss, *Robotic friction stir welding*, *Industrial Robot: An International Journal*, vol 31(1), 2004, pp. 55-63.
- [22] A. Bres, B. Monsarrat, L. Dubourg, C. Perron, M. Jahazi, L. Birglen and L. Baron, *Simulation of friction stir welding using industrial robots*, *Industrial Robot: An International Journal*, vol 37(1), 2010, pp. 36-50.
- [23] M. Guillo and L. Dubourg, *Impact & improvement of tool deviation in friction stir welding: weld quality & real-time compensation on an industrial robot*, *Robotics and Computer-Integrated Manufacturing*, vol 39, 2016, pp. 22-31.

Localized Strength Restoration of Aluminum 5083 with Ceramic Particles via FSP

- [24] Monsarrat, S. Larose, P. Wanjara, Y. Fortin, G. Comeau and A. Yousefpour, *Industrialization of robotic FSW for refurbishing of aluminum cathodes*, Proceedings of the 11th International Symposium on Friction Stir Welding, Cambridge, UK, 2016.
- [25] P. Wanjara, B. Monsarrat, B. and S. Larose, *Gap tolerances allowance and robotic operational window for friction stir butt welding of AA6061*, Journal of Materials Processing Technology, vol 213(4), 2013, pp. 631-640.
- [26] P. Wanjara, B. Monsarrat and S. Larose, *Process operational windows and industrialization scenarios for assembly of large aluminium structures by robotic friction stir welding*. Canadian Aeronautics and Space Journal, vol 60 (3), 2014, pp. 1-12.

Localized Strength Restoration of Aluminum 5083 with Ceramic Particles via FSP

